

Relativistic symmetry breaking in light kaonic nuclei

Rong-Yao Yang¹, Wei-Zhou Jiang¹, Qian-Fei Xiang², Dong-Rui Zhang¹, Si-Na Wei¹

¹*Department of Physics, Southeast University, Nanjing 210000, China*

²*Institute of High Energy Physics, Chinese Academy of Sciences, Beijing 100049, China*

As the experimental data from kaonic atoms and K^-N scatterings imply that the K^- -nucleon interaction is strongly attractive at saturation density, there is a possibility to form K^- -nuclear bound states or kaonic nuclei. In this work, we investigate the ground-state properties of the light kaonic nuclei with the relativistic mean-field theory. It is found that the strong attraction between K^- and nucleons reshapes the scalar and vector meson fields, leading to the remarkable enhancement of the nuclear density in the interior of light kaonic nuclei and the manifest shift of the single-nucleon energy spectra and magic numbers therein. As a consequence, the pseudospin symmetry is shown to be violated together with enlarged spin-orbit splittings in these kaonic nuclei.

PACS numbers: 13.75.Jz, 21.10.Dr, 21.10.Pc, 21.60.Gx

I. INTRODUCTION

The pseudospin symmetry (PSS), manifested by the quasidegeneracy between single-nucleon states with quantum numbers $(n, l, j = l + 1/2)$ and $(n - 1, l + 2, j = l + 3/2)$, was found more than 40 years ago [1, 2]. Subsequently, substantial efforts had been devoted to understanding the dynamic origin of the PSS until it was recognized that the PSS is a symmetry hidden in the equations for the small component of Dirac spinors. This might be natural and became clear later on since the relativistic mean-field (RMF) models are characteristic of the dynamical description of the spin degree of freedom and spin-orbit interactions [3–9]. The exact PSS is a consequence of the fact that the scalar and vector potentials are equal in size but opposite in sign, i.e., $\Sigma(r) = S(r) + V(r) = 0$, while in practice the PSS is approximate since the condition $\Sigma(r) = 0$ gives no bound state as in the RMF theory. However, the exception was found in Ref. [10] when the confining potential exists. In the Schrödinger-like equation for the small component of the Dirac spinor, the term proportional to $d\Sigma(r)/dr$ is related to the breaking of the PSS, and the small magnitude of that term gives the approximate PSS. For further understanding the properties of the PSS, people have studied the PSS in a number of physical processes and phenomena including superdeformation [9], nucleon-nucleon and nucleon-nucleus scatterings [11, 12], single particle resonant states [13], superheavy magic structures [14], identical bands [15], and pseudospin partner bands [16, 17], and so on.

The PSS breaking, proportional to the radial gradient of the potential $\Sigma(r)$, can vary with the isospin and charge of nuclei through the vector potential entry [6, 7, 18–20]. In the past, the PSS breaking had been studied extensively, and some very useful tools were also developed to analyze the breaking [13, 21, 22]. In addition to the isospin effects on the PSS breaking, the variation of the isoscalar potentials can also become one PSS breaking source, although this variation in different normal nuclei in the nuclear chart is not significant. In this work, our attention to the PSS breaking is focused on the exotic systems, the kaonic nuclei that may feature a characteristic enhancement of

the isoscalar density in the core of nuclei.

By analyzing experimental data of kaonic atoms and K^-N scatterings, people have found that K^-N interaction is strongly attractive at saturation density but with an optical potential depth roughly ranging from 40 to 200 MeV [23–34]. The great interest in studying kaonic nuclei has been attracted by the fact that the same sign of the vector and scalar potentials of the K^- creates a strong attraction that may lead to high-density K^- -nuclear bound states. In the past, lots of theoretical works have flourished. For instance, few-body calculations [34–38], the RMF and non-relativistic Skyrme-Hartree-Fock researches [26, 27, 39–41], were performed to obtain the K^- binding energy, the width and ground-state properties of K^- -nuclear bound states. Along with various predictions, experiments for the K^- bound states have also been progressive with the construction of new facilities[42–50].

Though the PSS is one of fundamental nuclear properties, it has not received due attention in kaonic nuclei. Indeed, the PSS has seldom been examined in kaonic nuclei. Thus, it is the aim of this work to investigate how the PSS is affected by the strong K^- -nucleon attraction in the RMF theory. For completeness and comparison, we will also examine the corresponding effect on spin-orbit splittings that are associated with the spin symmetry. The paper is organized as follows. The RMF formalism for kaonic (K^-) nuclei is given in Section II, and the pseudospin and spin symmetries in RMF are briefly manifested in section III. The results and discussions are given in section IV, followed by a brief summary in section V.

II. RMF FORMALISM FOR KAONIC NUCLEI

The relativistic Lagrangian containing K^- -nucleon interaction can be written as

$$\begin{aligned} \mathcal{L} = & \bar{\psi}_B [i\gamma_\mu \partial^\mu - M_B + g_{\sigma B} \sigma - g_{\omega B} \gamma_\mu \omega^\mu - g_{\rho B} \gamma_\mu \tau_3 b_0^\mu - e \frac{1 + \tau_3}{2} \gamma_\mu A^\mu] \psi_B \\ & - \frac{1}{4} F_{\mu\nu} F^{\mu\nu} + \frac{1}{2} m_\omega^2 \omega_\mu \omega^\mu - \frac{1}{4} B_{\mu\nu} B^{\mu\nu} + \frac{1}{2} m_\rho^2 b_{0\mu} b_0^\mu \\ & - \frac{1}{4} A_{\mu\nu} A^{\mu\nu} + \frac{1}{2} (\partial_\mu \sigma \partial^\mu \sigma - m_\sigma^2 \sigma^2) - \frac{1}{3} g_2 \sigma^3 - \frac{1}{4} g_3 \sigma^4 + \mathcal{L}_K, \end{aligned} \quad (1)$$

where ψ_B , σ , ω_μ , and $b_{0\mu}$ are the fields of the baryon, scalar, vector, and charge-neutral isovector-vector mesons, with their masses M_B , m_σ , m_ω , m_ρ , respectively. The A_μ is the field of photon. The g_{iB} ($i = \sigma, \omega, \rho$) are the corresponding meson-baryon coupling constants. The τ_3 is the third component of isospin Pauli matrix for nucleons. $F_{\mu\nu}$, $B_{\mu\nu}$, and $A_{\mu\nu}$ are the strength tensors of the ω , ρ meson and the photon, respectively

$$F_{\mu\nu} = \partial_\mu \omega_\nu - \partial_\nu \omega_\mu, \quad B_{\mu\nu} = \partial_\mu b_{0\nu} - \partial_\nu b_{0\mu}, \quad A_{\mu\nu} = \partial_\mu A_\nu - \partial_\nu A_\mu.$$

\mathcal{L}_K , the lagrangian of the kaonic sector [40, 51], is written as

$$\mathcal{L}_K = (\mathcal{D}_\mu K)^\dagger (\mathcal{D}^\mu K) - (m_K^2 - g_{\sigma K} m_K \sigma) K^\dagger K, \quad (2)$$

where the covariant derivative is given by

$$\mathcal{D}_\mu \equiv \partial_\mu + ig_{\omega K} \omega_\mu + ig_{\rho K} b_{0\mu} + ie \frac{1 + \tau_3}{2} A_\mu, \quad (3)$$

with the g_{iK} ($i = \sigma, \omega, \rho$) being the corresponding K^- -meson coupling constants. Here, K and K^\dagger denote the kaon and antikaon doublet, i.e. $K = \begin{pmatrix} K^- \\ K^0 \end{pmatrix}$ and $K^\dagger = (K^-, \bar{K}^0)$, respectively. Since our investigation is limited to K^- nuclei, the K^0 and \bar{K}^0 are left out in the following.

The equations of motion are derived from the Lagrangian (1). In the RMF approximation, the nucleons obey the following equation

$$[-i\vec{\alpha} \cdot \vec{\nabla} + \beta(M_B - g_{\sigma B} \sigma_0) + g_{\omega B} \omega_0 + g_{\rho B} \tau_3 b_0 + e \frac{1 + \tau_3}{2} A_0] \psi_B = E_B \psi_B. \quad (4)$$

In spherical systems we consider in this work, the equations of motion for non-strange mesons are given by

$$\begin{aligned} \left(\frac{d^2}{dr^2} + \frac{2}{r} \frac{d}{dr} - m_\sigma^2 \right) \sigma_0 &= g_{\sigma B} \rho_s - g_2 \sigma_0^2 - g_3 \sigma_0^3 + g_{\sigma K} m_K K^- K^+, \\ \left(\frac{d^2}{dr^2} + \frac{2}{r} \frac{d}{dr} - m_\omega^2 \right) \omega_0 &= g_{\omega B} \rho_v - g_{\omega K} \rho_{K^-}, \\ \left(\frac{d^2}{dr^2} + \frac{2}{r} \frac{d}{dr} - m_\rho^2 \right) b_0 &= g_{\rho B} \rho_3 - g_{\rho K} \rho_{K^-}, \\ \left(\frac{d^2}{dr^2} + \frac{2}{r} \frac{d}{dr} \right) A_0 &= e \rho_p - e \rho_{K^-}, \end{aligned} \quad (5)$$

where ρ_s , ρ_v , ρ_p and ρ_3 are the scalar, vector, proton, and isovector densities, respectively, and we refer readers to Ref. [52, 53] for detailed expressions. The ρ_{K^-} denotes the K^- density

$$\rho_{K^-} = 2(E_{K^-} + g_{\omega K} \omega_0 + g_{\rho K} b_0 + e A_0) K^- K^+, \quad (6)$$

where the integration of ρ_{K^-} over the whole volume is normalized to the K^- number which is one in this work. The Klein-Gordon equation for K^- reads

$$(\nabla^2 + E_{K^-}^2 - m_K^2 - \Pi) K^- = 0, \quad (7)$$

where E_{K^-} is the single-particle energy of the K^- . The real part of the K^- self-energy Π is written as

$$\begin{aligned} \Re \Pi &= -g_{\sigma K} m_K \sigma_0 - 2E_{K^-} (g_{\omega K} \omega_0 + g_{\rho K} b_0 + e A_0) \\ &\quad - (g_{\omega K} \omega_0 + g_{\rho K} b_0 + e A_0)^2. \end{aligned} \quad (8)$$

The imaginary part $\Im \Pi$ is considered as the absorptive contribution to the K^- self-energy which can be taken from some optical models phenomenologically. Following works of Mareš et al. [26, 27], we adopt the simple 't ρ ' form $\Im \Pi = f V_0 \rho_v(r)$ where the depth V_0 is obtained by fitting K^- atomic data [24].

III. REVISIT TO THE RELATIVISTIC SYMMETRY MANIFESTATION IN RMF

The concept of PSS is introduced to describe the quasidegeneracy in some nuclei between single-nucleon states with quantum numbers $(n, l, j = l + 1/2)$ and $(n - 1, l + 2, j = l + 3/2)$, e.g., $2S_{1/2}$ and $1D_{3/2}$. The PSS can be understood as a relativistic symmetry of the Dirac Hamiltonian originating from the near equality in magnitude of the scalar potential $S(r)$ and vector potential $V(r)$ but different in sign, i.e. $S(r) + V(r) \approx 0$ [5]. The quality of the approximate symmetry was found to be associated with the competition between pseudocentrifugal barrier and the pseudospin-orbit potential [6, 7]. In the following, we demonstrate in the RMF the conditions for the PSS.

Since the meson fields are classical in the RMF, one can write the Dirac Hamiltonian for nucleons in spherical nuclei as

$$\hat{h} = -i\vec{\alpha} \cdot \vec{\nabla} + g_{\omega B}\omega_0 + g_{\rho B}\tau_3 b_0 + e\frac{1 + \tau_3}{2}A_0 + \beta(M_B - g_{\sigma B}\sigma_0). \quad (9)$$

It is well-known that the total angular momentum \mathbf{J} commutes with the Hamiltonian and is a conserved operator. While the orbital angular momentum \mathbf{L} does not commute with the \hat{h} , to characterize the full set of quantum numbers of single-particle states, one invokes another conserved operator \mathbf{K}

$$\mathbf{K} \equiv -\gamma^0(\boldsymbol{\Sigma} \cdot \mathbf{L} + 1), \quad (10)$$

with its eigenvalues

$$\kappa = \begin{cases} l, & j = l - \frac{1}{2}, \\ -(l + 1), & j = l + \frac{1}{2}. \end{cases} \quad (11)$$

Then we have $j = |\kappa| - 1/2$ and $l = |\kappa| + (\kappa/|\kappa| - 1)/2$. For a spherical system, the quantum number set is $\{n, \kappa, m, t\}$ where n is the principle quantum number, m is the magnetic quantum number, and t denotes the isospin. With these quantum numbers, the single-particle wave functions can be written as

$$\psi_{n\kappa mt}(r) = \left\{ \begin{array}{c} i\frac{G_a(r)}{r}\Phi_{\kappa, m} \\ -\frac{F_a(r)}{r}\Phi_{-\kappa, m} \end{array} \right\} \chi_t, \quad (12)$$

where $G_a(r)$ and $F_a(r)$ are the big and small components of the (radial) spinor, respectively, $\{a\} = \{n, \kappa, t\}$, Φ is the spinor spherical harmonic, and χ_t is the isospinor with $t = \pm 1$ for protons and neutrons, respectively. Substituting Eq. (12) into the Dirac equation (4), one can immediately obtain the radial equations for nucleons

$$\left(\frac{d}{dr} + \frac{\kappa}{r}\right)G_a(r) = (M_B + E_a - \Delta)F_a(r), \quad (13)$$

$$\left(\frac{d}{dr} - \frac{\kappa}{r}\right)F_a(r) = (M_B - E_a + \Sigma)G_a(r), \quad (14)$$

where

$$\Sigma = V(r) + S(r), \quad \Delta = V(r) - S(r), \quad (15)$$

with $V(r) = g_{\omega B}\omega_0 + g_{\rho B}\tau_3 b_0 + eA_0(1 + \tau_3)/2$ and $S(r) = -g_{\sigma B}\sigma_0$. By performing radial derivative on the both sides of Eq. (13) and (14), one arrives at the two second-order differential equations for the big and small components, respectively

$$\left[\frac{d^2}{dr^2} + \frac{1}{U_G} \frac{d\Delta}{dr} \frac{d}{dr} + \frac{1}{U_G} \frac{d\Delta}{dr} \frac{\kappa}{r} - \frac{\kappa(\kappa+1)}{r^2} - U_G U_F \right] G_a(r) = 0, \quad (16)$$

$$\left[\frac{d^2}{dr^2} - \frac{1}{U_F} \frac{d\Sigma}{dr} \frac{d}{dr} + \frac{1}{U_F} \frac{d\Sigma}{dr} \frac{\kappa}{r} - \frac{\kappa(\kappa-1)}{r^2} - U_G U_F \right] F_a(r) = 0, \quad (17)$$

with $U_G = M_B + E_a - \Delta$ and $U_F = M_B - E_a + \Sigma$. These two equations are equivalent for obtaining the eigenvalues E_a . Similar to the description in Ref. [6], the centrifugal barrier (CB) and pseudocentrifugal barrier (PCB) are here defined as $\kappa(\kappa+1)/r^2$ and $\kappa(\kappa-1)/r^2$, respectively. The spin-orbit potential (SOP) and pseudospin-orbit potential (PSOP) terms are those in Eqs.(16) and (17) proportional to $\kappa d\Delta/(rdr)$ and $\kappa d\Sigma/(rdr)$, respectively. If the SOP term equals exactly to zero, say, $\Delta = 0$ or $d\Delta/dr = 0$, it can be obviously seen from Eq. (16) that the eigenvalue E_a only depends on $\kappa(\kappa+1)$. One can easily find out that those states with $\kappa = l$ and $\kappa = -(l+1)$ share the same eigenvalues. This is nothing but the spin symmetry leading to the spin degeneracy. Similarly, if the PSOP term equals exactly to zero, say, $\Sigma = 0$ or $d\Sigma/dr = 0$, then the eigenvalue E_a only depends on $\kappa(\kappa-1)$ as seen from Eq. (17). Introducing $\tilde{l} = l+1$, we can see that those states with $\kappa = -\tilde{l}$ and $\kappa = \tilde{l}+1$ have the same eigenvalues. This type of degeneracy was named the PSS in resemblance to the spin symmetry. However, the PSS is nonexistent once the PSOP term is far away from zero. Generally speaking, as already pointed out in Ref. [6], the quality of the PSS is tightly associated with the relative magnitude of PCB to the PSOP in the RMF, while the correlation between PSOP term and the PSS is not simply linear [54].

In a normal nuclear system, the attractive potential is usually around 380MeV, while the repulsion is around 320MeV. It gives rise to $\Delta \approx 700$ MeV, corresponding to relative large SOP term, while the Σ is around -60 MeV, leading to a relative small PSOP term. This estimation indicates that the PSS is developed much better than the spin symmetry in normal nuclear single-particle spectra. In plenty of nuclei, the PSS exists approximately and the splitting of pseudospin doublets $(n, l, j = l + 1/2)$ and $(n - 1, l + 2, j = l + 3/2)$ is relatively small, compared to the separation between two levels nearby. But the appearance of K^- could change the proportion of the attraction to the repulsion, leading to the alteration of Δ and Σ . Thus, the general situation for the PSS in kaonic nuclei can be rather different and it is worthy of careful investigations.

IV. RESULTS AND DISCUSSIONS

As one source term of the mean field, the K^- diminishes its role in the mean field with the increase of the nuclear mass. Thus, our investigation is limited to the medium and light nuclei in which the K^- has more distinct effects on nuclear properties, especially the bulk density of the nuclear system and the single-particle energy for the pseudospin and spin doublets. We perform calculations with the NL3 parameter set [55]. The $g_{\omega K}$ and $g_{\rho K}$ are chosen from SU(3) relations: $2g_{\omega K} = 2g_{\rho K} = g_{\rho\pi} = 6.04$, and the $g_{\sigma K}$ is adjusted to yield a K^- binding energy $B_{K^-} = 100\text{MeV}$ for ${}^{40}_{K^-}\text{Ca}$ where the B_{K^-} is defined as the difference of the total binding energy between the kaonic nucleus and its normal counterpart without K^- . Though the moderately deep optical potential is adopted here ($\approx 100\text{ MeV}$), as in some pioneer works [39–41], we will examine the cases for various binding energies at last. The coupled equations (5),(7), (13) and (14) are solved self-consistently by an iterative procedure. Some details of solving the K^- equation are given in the Appendix.

TABLE I: Single-neutron binding energies and splittings of the pseudospin and spin doublets in normal nuclei and the corresponding kaonic nuclei (in unit of MeV) with the NL3.

	$2S_{1/2}$	$1D_{3/2}$	Δ (2S-1D)	$1D_{5/2}$	Δ (1D)	$1P_{3/2}$	$1P_{1/2}$	Δ (1P)
${}^{16}\text{O}$	-	-	-	-	-	21.73	15.25	6.48
${}^{16}_{K^-}\text{O}$	-	-	-	-	-	27.43	6.75	20.68
${}^{34}\text{S}$	13.95	10.45	3.50	18.59	8.14	35.85	28.82	7.03
${}^{34}_{K^-}\text{S}$	20.81	8.45	12.36	18.85	10.40	40.18	24.52	15.66
${}^{40}\text{Ca}$	16.96	16.17	0.79	22.88	6.71	37.98	33.50	4.48
${}^{40}_{K^-}\text{Ca}$	25.86	14.49	11.37	23.19	8.70	41.57	30.94	10.63
${}^{48}\text{Ca}$	17.56	17.73	-0.17	23.88	6.15	38.94	35.63	3.31
${}^{48}_{K^-}\text{Ca}$	21.36	16.77	4.59	25.00	8.23	42.61	36.48	6.13
${}^{52}\text{Cr}$	20.21	21.89	-1.68	27.95	6.06	42.95	40.11	2.84
${}^{52}_{K^-}\text{Cr}$	22.95	21.44	1.51	29.52	8.08	46.80	42.12	4.68
${}^{58}\text{Ni}$	22.85	26.08	-3.23	31.38	5.30	45.71	43.67	2.04
${}^{58}_{K^-}\text{Ni}$	25.10	26.22	-1.12	33.23	7.01	49.59	46.41	3.18
${}^{74}\text{Se}$	25.63	29.42	-3.79	33.55	4.13	45.21	43.41	1.80
${}^{74}_{K^-}\text{Se}$	28.05	29.78	-1.73	34.90	5.12	47.93	45.40	2.53
${}^{90}\text{Zr}$	30.29	32.43	-2.14	36.32	3.89	48.38	46.56	1.82
${}^{90}_{K^-}\text{Zr}$	33.35	32.62	0.73	37.46	4.84	51.02	48.14	2.88

Tabulated in Table I are the single-neutron binding energies and the splittings of pseudospin and spin doublets for a few states in some spherical nuclei and in the corresponding kaonic nuclei. Those results for protons are not presented here because of no qualitative difference therein. Seen from this table, the most noticeable change of the single-particle binding energy in these kaonic nuclei is the considerable increase in the binding energy of the $2S_{1/2}$ and $1P_{3/2}$ states while just a little effect

on $1D_{3/2}$, especially for those light nuclei. For instance, in ^{40}Ca , the pseudospin doublets $2S_{1/2}$ and $1D_{3/2}$ are very close, showing that the PSS is satisfied approximately, whereas the situation is quite different when the K^- is implanted into ^{40}Ca . The big separation between the corresponding doublets arises in $^{40}_{K^-}\text{Ca}$ due to a dramatic increase of the binding energy of the $2S_{1/2}$ state while a small reduction in $1D_{3/2}$, leading to the manifest breaking of the PSS. Besides in $^{40}_{K^-}\text{Ca}$, similar orbital shifts take place in other kaonic nuclei as seen in Table I. Interestingly, with the increase of the nucleon number, the orbital shifts in heavier nuclei $^{58}_{K^-}\text{Ni}$, $^{74}_{K^-}\text{Se}$, and $^{90}_{K^-}\text{Zr}$ even favor the approximate PSS, being more satisfactory than those in corresponding normal nuclei. This takes place because the shallower binding of the $2S_{1/2}$ state in the pseudospin doublet of heavier nuclei accompanies with the smaller binding enhancement of such a state in corresponding kaonic nuclei. On the other hand, the spin-orbit splittings between $1P_{3/2}$ and $1P_{1/2}$ all get a rise in kaonic nuclei listed in Table I. For instance, the energy interval between $1P_{3/2}$ and $1P_{1/2}$ is 4.48 MeV for ^{40}Ca , while it is 10.63 MeV for $^{40}_{K^-}\text{Ca}$. Needless to say, the breaking of the spin symmetry becomes more distinctive in these kaonic nuclei, in comparison to that in normal nuclei. We mention that the effect of the imaginary part of K^- on the nuclear density and single-particle energies is insignificant for the given K^- binding energy 100 MeV, and it just becomes moderate for much weaker binding energies. Thus, we will not regard it specifically in the following discussion.

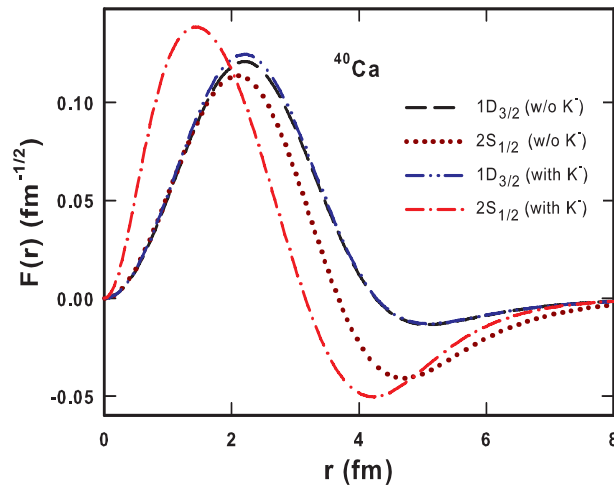


FIG. 1: (Color online) The small components of the Dirac spinor for neutrons in ^{40}Ca and $^{40}_{K^-}\text{Ca}$ as a function of radius. Those labelled "w/o K^- " and "with K^- " represent for normal nuclei and corresponding kaonic nuclei, respectively, and we will keep these abbreviations throughout.

Now, we take ^{40}Ca and $^{40}_{K^-}\text{Ca}$ as a typical example to understand the PSS features in kaonic nuclei. In Fig. 1, we plot the small components of the Dirac spinor, i.e. $F_a(r)$. As discussed in Sec.III, the similarity in the small components of the Dirac spinor is associated with the approximate PSS [56]. Indeed, this is the case in ^{40}Ca : the $F(r)$ s for the pseudospin doublets $2S_{1/2}$ (dotted curve) and $1D_{3/2}$

(dashed curve) are rather close, though one has a node and the other without. But the addition of the K^- in ^{40}Ca forces the small component of the $2S_{1/2}$ state to move inwards considerably. As a result, the breaking of the PSS appears with the similarly explicit shift in the small component of the Dirac spinor. While with the increase of the nuclear number, the relative shift of $F(r)$ in kaonic nuclei becomes trivial, consistent with the much smaller shift in single-particle binding energy.

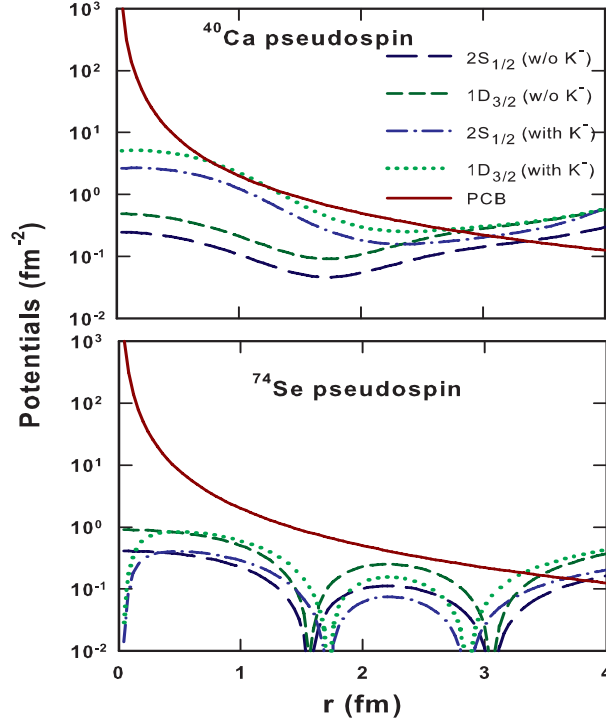


FIG. 2: (Color online) The PCBs and PSOPs (denoted by orbital quanta) in Eq. (17) for pseudospin doublets $2S_{1/2}$ and $1D_{3/2}$ in ^{40}Ca and ^{74}Se systems. Also see text.

For a deeper understanding of these phenomena concerning the addition of the K^- , we illustrate in Fig. 2 the radial distributions of some relevant potential terms for pseudospin doublets ($2S_{1/2}$ and $1D_{3/2}$) in ^{40}Ca , ^{74}Se and in the corresponding kaonic nuclei. They are the PCB $|\kappa(\kappa-1)|/r^2$ and the PSOP $|\kappa d\Sigma/U_F r dr|$, see Eq. (17). Because the K^- is trapped in the interior nutshell by the strong attraction and its effect becomes insignificant beyond $r = 4fm$, only shown in the figure are the results in the region $r \leq 4fm$ for clarity. The relative magnitude of the PCB to the PSOP, closely associated with the quality of the PSS, can be used to evaluate the extent of the corresponding symmetry breaking. It is seen from the upper panel of Fig. 2 that PSOP is largely enhanced by the K^- in $^{40}_{K^-}\text{Ca}$, especially in the region $r \lesssim 2fm$. Due to the large enhancement, the PSOP and PCB in $^{40}_{K^-}\text{Ca}$ are comparable. It is now not difficult for us to understand why the PSS is destroyed in $^{40}_{K^-}\text{Ca}$: the clear enhancement of the PSOP brings out the importance of the κ dependence of eigen energies and vectors (wave functions) that is the exact factor for the PSS breaking, see Eq. (17).

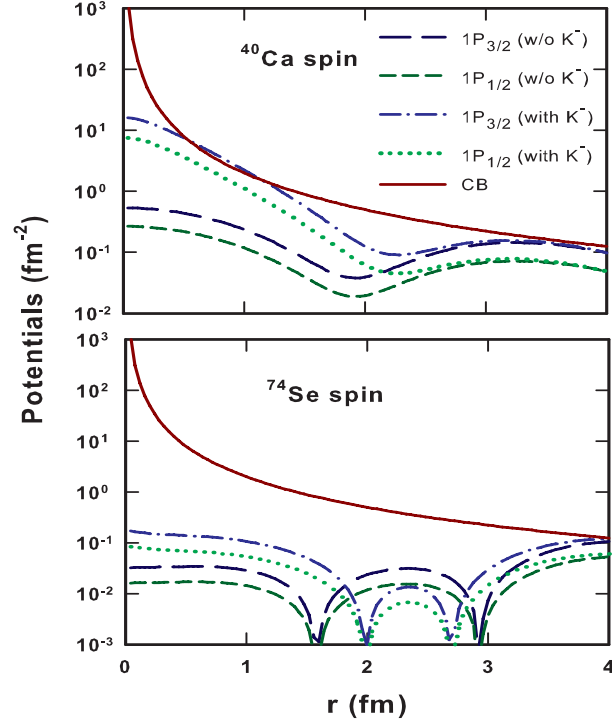


FIG. 3: (Color online) The CBs $|\kappa(\kappa - 1)|/r^2$ and SOPs $|\kappa d\Sigma/U_{Fr}dr|$ (labelled by orbital quanta), see Eq. (16), for spin doublets $1P_{1/2}$ and $1P_{3/2}$ in ^{40}Ca and ^{74}Se systems.

We have already seen in Table I that the PSS in $^{74}_{K^-}\text{Se}$ is a little better than that in ^{74}Se . It is again illustrated in terms of the corresponding potentials for ^{74}Se and $^{74}_{K^-}\text{Se}$ in the lower panel of Fig. 2 that the PSOP is small compared to the PCB and is much less affected by the K^- , which justifies the approximate PSS both in ^{74}Se and $^{74}_{K^-}\text{Se}$. We may further examine the potentials in ^{74}Se and $^{74}_{K^-}\text{Se}$ in more details. For $r \lesssim 1.6\text{fm}$, the PSOP difference between ^{74}Se and $^{74}_{K^-}\text{Se}$ is not significant, while in the range of $1.6\text{fm} \lesssim r \lesssim 2.8\text{fm}$, the PSOP of ^{74}Se is clearly larger than that of $^{74}_{K^-}\text{Se}$. The latter may be responsible for the improvement of the PSS in $^{74}_{K^-}\text{Se}$, as this is consistent with the situation in heavier nuclei that more nucleons in exterior shells produce the more radial extension of the K^- by the attraction. In general, the difference in the PSOP caused by the K^- embedment becomes small in heavy nuclei, and distinctive features with the embedment of the K^- tend to disappear.

The situation for the shift of spin-orbit splitting is quite analogous. The attraction provided by the K^- leads to the deepening of the SOP, and the κ dependence of eigenvalues of the spin doublets is magnified. For heavier and heavier nuclei, the K^- effect on the spin-orbit splitting drops off, just like the case of the PSS breaking. These phenomena are clearly shown in Fig. 3, in resemblance to the pseudospin case in Fig. 2, and are consistent with those for the spin-orbit splittings listed in Table I.

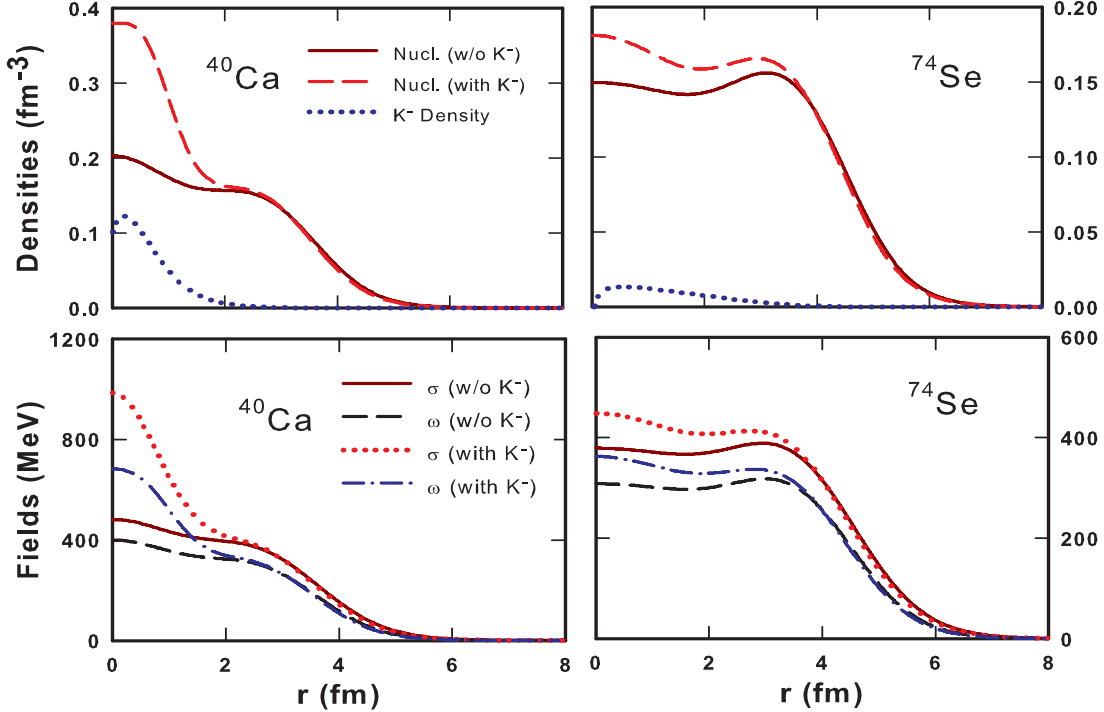


FIG. 4: (Color online) Nuclear densities and potentials as a function of radius in ^{40}Ca (left panels) and ^{74}Se systems (right panels).

The most striking phenomenon of the kaonic nuclei should be the enhancement of the central density [39–41]. The enhancement in light nuclei could be very prominent. Here, we take ^{40}Ca and comparably ^{74}Se systems as examples. In Fig. 4, it displays the radial distributions of the densities and potentials. For ^{40}Ca systems, we see that the K^- is deeply bound inside the interior of the kaonic nuclei ($r \lesssim 2\text{fm}$) due to the strong attraction. This deeply trapped K^- distribution is consistent with the sizeable rise of the SOP and PSOP in the core region, as shown in Fig. 2 and 3, respectively. As a result, the strong attraction provided by the K^- in ^{40}Ca pulls nucleons inwards to form a dense core with a density up to twice the saturation density, as shown in the upper left panel of Fig. 4. We recall that the strong attraction responsible for this is produced by the coherent coupling of σ and ω mesons to the K^- . Feeding back to the mean field in kaonic nuclei, the attractive potential ($g_\sigma\sigma$) in the shrunk core acquires an enhancement greater than the one for the repulsive potential ($g_\omega\omega$), as clearly shown in the lower left panel in Fig. 4. The enhancement of the core density also exists in all the kaonic nuclei, while it fades away gradually in heavy nuclei. Shown in the right panels of Fig. 4 is the case for ^{74}Se systems. As can be seen, the K^- is pulled outwards by the attraction provided by more out-layer nucleons. As a consequence, just moderate increase of the core density and mean-field potentials in $^{74}_{K^-}\text{Se}$, instead of the dramatic increase in light nuclei, is observed. Consistently, the shifts of single-particle energy are much smaller than those in light

nuclei. We note that the calculations with the non-relativistic Skyrme-Hartree-Fock approach also found the similar shrinkage [41]. These results are inspiring as kaonic nuclei could probably provide a natural cold dense nuclear system rather than a hot dense one that should be created by heavy-ion collisions.

Besides the above general analysis for the PSS breaking, we have not paid much attention to a specific phenomenon, the almost unilateral shift of the pseudospin doublets. Looking back to Fig. 1, we see that it is the shift of the $2S_{1/2}$, rather than that of the $1D_{3/2}$, which dominates the PSS breaking. This can be roughly understood by the spatial proximity between the $1S_{1/2}$ K^- and $2S_{1/2}$ nucleons. To make it clear, we plot the simple product between the neutron wave function square of different states in ^{40}Ca and K^- density distribution in $^{40}_{K^-}\text{Ca}$ in Fig. 5. We see that unlike the $S_{1/2}$ orbitals, the $1D$ orbitals are almost uncorrelated with the K^- occupation. This illustrates why the $2S_{1/2}$ state of pseudospin doublets is affected much more dramatically by the K^- . Further, this is associated with the change of the shell structure. Shown in Fig. 6 is the single-particle spectra for protons and neutrons in ^{42}Ca and $^{42}_{K^-}\text{Ca}$. It is clearly shown that the K^- implantation leads the migration of $1S_{1/2}$ and $2S_{1/2}$ nucleons downwards to the deep Fermi sea. The orbital migration certainly changes the original magic numbers in normal nuclei that are 2, 8, 20... In $^{42}_{K^-}\text{Ca}$, the magic numbers now become 2, 6 and 16 that are dictated by the migrated $S_{1/2}$ orbitals and enlarged spin-orbit splittings of $1P$ and $1D$ orbitals, as shown in Fig. 6. Though it is perhaps premature to speak of the new magic numbers because the magic gaps should rely on the depth of the potential well for the K^- , it is definite that the nuclear structure is changed by the K^- implantation.

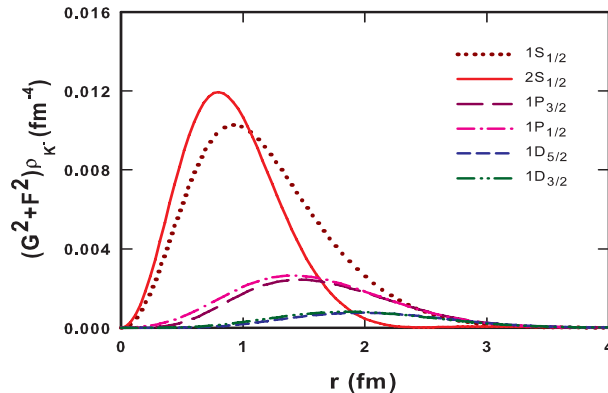


FIG. 5: (Color online) Products of the square of various neutron wave functions in ^{40}Ca and K^- density distribution in $^{40}_{K^-}\text{Ca}$.

By now, there is no conclusive value of the depth of the K^- -nuclear potential. Thus, it is valuable to investigate the dependence of energy splittings of the pseudospin and spin doublets on the K^- binding energy. Specifically, we obtain various splittings of pseudospin and spin doublets by changing

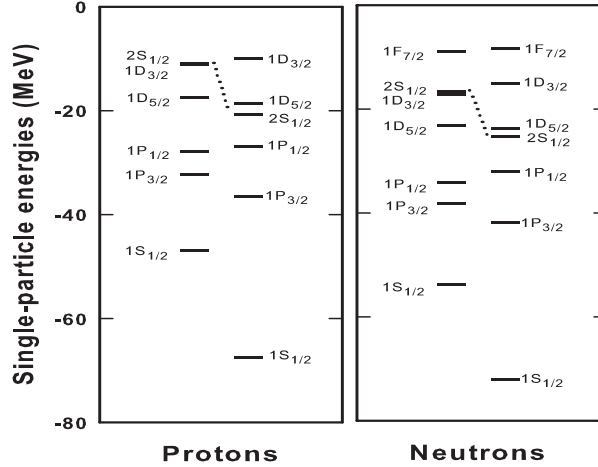


FIG. 6: Single-particle energies in ^{42}Ca and $^{42}_{K^-}\text{Ca}$. The left column in each panel represents energy levels for ^{42}Ca , while the right ones are for $^{42}_{K^-}\text{Ca}$.

$g_{\sigma K}$ and $g_{\omega K}$, which is equivalent to varying the K^- binding energy. Results are displayed in Fig. 7 for the pseudospin doublets ($2S_{1/2}$ and $1D_{3/2}$), ($1P_{1/2}$ and $1P_{3/2}$) and ($1D_{3/2}$ and $1D_{5/2}$). At the point $B_{K^-}=0$, i.e. the normal ^{40}Ca , the pseudospin doublet splitting between $2S_{1/2}$ and $1D_{3/2}$ is less than 1 MeV. The splitting becomes increasingly large with the enhancement of the K^- -nuclear attraction, while a clear increase appears at $B_{K^-} > 80\text{MeV}$. Similarly, the splitting of the spin doublets $1P_{1/2}$ and $1P_{3/2}$ is apparently amplified by increasing the K^- -nuclear attraction. We see that the effect on the doublet $1D_{3/2}$ and $1D_{5/2}$ is relatively smaller. This is understandable since the out-layer states are less affected by the interior K^- . Nevertheless, larger K^- binding can generally result in more prominent phenomenon of the pseudospin and spin symmetry breakings, especially for interior states.

The above discussion on the association between the doublet splittings and the K^- binding energy also leads our attention to more details of the model dependence. We find that the splittings of the pseudospin and spin doublets are almost independent of various combinations of different $g_{\sigma K}$ and $g_{\omega K}$ for a given K^- binding energy. While we change to other models like the NL-SH [57], we find that the size of the doublet splittings is quantitatively different not only due to various incompressibility at saturation density but also because of the rather different equations of state at suprasaturation densities. Nevertheless, the splittings are still very large for light kaonic nuclei. Moreover, we should point out that all results with the NL-SH are qualitatively similar to those obtained from the NL3, without changing the conclusions drawn above.

At last, it is worthy to point out the dependence of the spin or pseudospin doublet splittings on the isospin. With the increase of the neutron number, the repulsion provided by the isovector

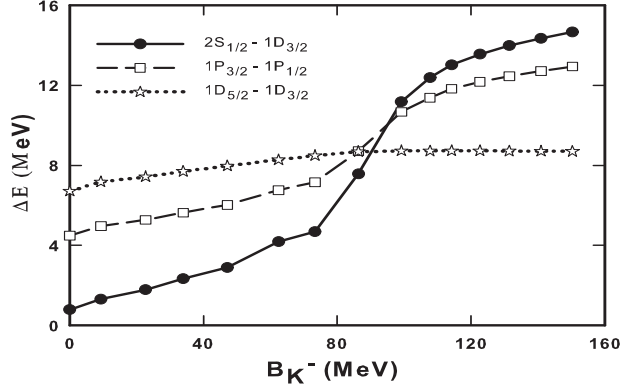


FIG. 7: Splittings of pseudospin and spin doublets in $^{40}_{K^-}\text{Ca}$ as a function of K^- binding energy. $B_{K^-}=0$ represents normal ^{40}Ca .

meson increases. This causes the moderate reduction of the relevant doublet splittings. However, the splittings are still well above those for the normal nuclei.

V. SUMMARY

We have investigated the ground-state properties of light kaonic nuclei and the relativistic symmetry breakings with the RMF model. It is found that the relativistic symmetry breakings, underlying potentials associated with the breakings, and the appreciable shrinkage effect, i.e., the significantly enhanced core density take place consistently due to the strong attraction provided by the K^- embedment in light nuclei. For normal nuclei entertaining the approximate pseudospin symmetry, the K^- embedment can enhance κ -dependence of the eigen energies and wave functions, break the original balance between the attractive and repulsive potentials consequently, and result in the pseudospin symmetry breaking and the spin symmetry deterioration. With the K^- embedment, the shell structures are also changed dramatically in light nuclei. In particular, the migration of $S_{1/2}$ orbitals towards the interior Fermi sea and the enlarged spin-orbit splittings can reshape the order of energy levels and form new magic numbers. Moreover, we have examined the dependence on the K^- binding energy and the model dependence for these phenomena. The model dependence is rather weak, and we find that for a large parameter space of the K^- binding energy all the phenomena are quite general.

Acknowledgements

We thank Prof. Xian-Hui Zhong for useful discussions. The work was supported in part by the National Natural Science Foundation of China under Grant No. 11275048, the China Jiangsu

Provincial Natural Science Foundation under Grant No.BK20131286, and the China Scholarship Council.

Appendix A: Solving the Klein-Gordon equation for K^-

We give some necessary details for solving the Klein-Gordon equation for K^- (Eq. 7) herein. Eq. (7) is a complex equation which should firstly be divided into two coupled real equations. In a spherical system, Eq. (7) can be written as

$$\left(-\frac{d^2}{dr^2} + \frac{l(l+1)}{r^2}\right)K^-(r) + M_K^2 + \Pi(r)K^-(r) = E^2K^-(r). \quad (\text{A1})$$

It is decomposed as

$$\left(\frac{d^2}{dr^2} + U_1(r)\right)K_{\Re}^-(r) - U_2(r)K_{\Im}^-(r) = 0, \quad (\text{A2})$$

$$\left(\frac{d^2}{dr^2} + U_1(r)\right)K_{\Im}^-(r) + U_2(r)K_{\Re}^-(r) = 0, \quad (\text{A3})$$

with $U_1(r) = -\frac{l(l+1)}{r^2} + E_{\Re}^2 - E_{\Im}^2 - M_K^2 - \Re\Pi(r)$, $U_2(r) = 2E_{\Re}E_{\Im} - \Im\Pi(r)$. These are second-order differential equations, and can be solved by the Runge-Kutta method, or the Numerov method. In this work, the Runge-Kutta method is adopted. Given the boundary values and a trial eigenvalue E_{tr} , we can integrate those equations from $r = 0$ outwards and from $r = \infty$ (far away enough) inwards to a match point $r = r_m$, and then connect the wave function at this point. By integrating the integrand that is $K_{tr}^{-*}(r)$ times Eq. (A1) in the range $0 < r < r_m - \epsilon$ and $r_m + \epsilon < r < \infty$ (ϵ is a positive infinitesimal), we can get

$$E_{tr}^2 = \int K_{tr}^{-*}(r)\left(-\frac{d^2}{dr^2} + \frac{l(l+1)}{r^2} + M_K^2 + \Pi(r)\right)K_{tr}^-(r)dr / \int K_{tr}^{-*}(r)K_{tr}^-(r)dr. \quad (\text{A4})$$

However, we must keep in mind that $dK^-(r)/dr$ is discontinuous at $r = r_m$ as long as E_{tr} is still not the eigenvalue. This discontinuity is used to adjust the eigenvalue in an iterative way $E_{tr}^2 = E_{tr}^2 + \Delta E_{tr}^2$ with ΔE_{tr}^2 being given as

$$\Delta E_{tr}^2 \approx \int_{r_m-\epsilon}^{r_m+\epsilon} -K_{tr}^{-*}(r)\frac{d^2K_{tr}^-(r)}{dr^2}dr / \int_0^{\infty} K_{tr}^{-*}(r)K_{tr}^-(r)dr \quad (\text{A5})$$

$$\approx -K_{tr}^{-*}(r_m)\left[\frac{dK_{tr}^-(r_m+\epsilon)}{dr} - \frac{dK_{tr}^-(r_m-\epsilon)}{dr}\right] / \int_0^{\infty} K_{tr}^{-*}(r)K_{tr}^-(r)dr, \quad (\text{A6})$$

where we have disregarded all infinitesimal terms in ϵ by considering that the remaining term is from the derivative of the discontinuity which embodies the property of the Dirac δ function.

[1] A. Arima, M. Harvey, and K. Shimizu, Phys. Lett. **30B**, 517 (1969).

[2] K. T. Hecht and A. Adler, Nucl. Phys. A **137**, 129 (1969).

[3] C. Bahri, J. P. Draayer, and S. A. Moszkowski, Phys. Rev. Lett. **68**, 2133 (1992).

- [4] A. L. Blokhin, C. Bahri, and J. P. Draayer, Phys. Rev. Lett. **74**, 4149 (1995).
- [5] J. N. Ginocchio, Phys. Rev. Lett. **78**, 436 (1997).
- [6] J. Meng et al, Phys. Rev. C **58**, R628 (1998).
- [7] J. Meng et al, Phys. Rev. C **59**, 154 (1999).
- [8] J. N. Ginocchio, Phys. Rep. **315**, 231 (1999).
- [9] J. Dudek, W. Nazarewicz, Z. Szymanski, and G. A. Leander, Phys. Rev. Lett. **59**, 1405 (1987).
- [10] P. Alberto, A. S. de Castro, M. Malheiro, Phys. Rev. C **87**, 031301(R) (2013).
- [11] J. N. Ginocchio, Phys. Rev. Lett. **82**, 4599 (1999).
- [12] J. N. Ginocchio, Phys. Rev. C **65**, 054002 (2002).
- [13] B. N. Lu, E. G. Zhao, and S. G. Zhou, Phys. Rev. Lett. **109**, 072501 (2012).
- [14] J. J. Li et al, Phys. Lett. B **732** 169 (2014).
- [15] W. Nazarewicz et al, Phys. Rev. Lett. **64**, 1654 (1990).
- [16] Q. Xu et al., Phys. Rev. C **78**, 064301 (2008).
- [17] W. Hua et al., Phys. Rev. C **80**, 034303 (2009).
- [18] P. Alberto et al, Phys. Rev. Lett. **86**, 5015 (2001).
- [19] S. Marcos et al, Phys. Lett. B **513**, 30 (2001).
- [20] R. Lisboa et al, Phys. Rev. C **81**, 064324 (2010).
- [21] H. Z. Liang et al, Phys. Rev. C **87**, 014334 (2013).
- [22] J. Y. Guo et al, Phys. Rev. Lett. **112**, 062502 (2014).
- [23] C. J. Batty, E. Friedman, and A. Gal, Phys. Rep. **287**, 385 (1997).
- [24] E. Friedman, A. Gal, J. Mareš, and A. Cieplý, Phys. Rev. C **60**, 024314 (1999).
- [25] A. Ramos, and E. Oset, Nucl. Phys. A **671**, 481 (2000).
- [26] J. Mareš, E. Friedman, and A. Gal, Phys. Lett. B **606**, 295 (2005).
- [27] J. Mareš, E. Friedman, and A. Gal, Nucl. Phys. A **770**, 84 (2006).
- [28] E. Friedman, A. Gal, and C. J. Batty, Phys. Lett. B **308**, 6 (1993).
- [29] E. Friedman, A. Gal, and C. J. Batty, Nucl. Phys. A **579**, 518 (1994).
- [30] S. Hirenzaki et al, Phys. Rev. C **61**, 055205 (2000).
- [31] A. Baca, C. García-Recio, and J. Nieves, Nucl. Phys. A **673**,335 (2000).
- [32] E. Friedman, and A. Gal, Phys. Rep. **452**, 89 (2007).
- [33] D. Gazda, and J. Mareš, Nucl. Phys. A **881**, 159 (2012).
- [34] Y. Akaishi, and T. Yamazaki, Phys. Rev. C **65**, 044005 (2002).
- [35] A. Gal, Nucl. Phys. A **914**, 270 (2013).
- [36] T. Yamazaki, and Y. Akaishi, Phys. Lett. B **353**, 70 (2002).
- [37] N. V. Shevchenko, A. Gal, and J. Mareš, Phys. Rev. Lett. **98**, 082301 (2007).
- [38] A. Doté, T. Hyodo, and W. Weise, Phys. Rev. C **79**, 014003 (2009).
- [39] X. H. Zhong et al, Phys. Rev. C **74**, 034321 (2006).
- [40] D. Gazda, E. Friedman, A. Gal, and J. Mareš, Phys. Rev. C **76**, 055204 (2007).
- [41] X. R. Zhou, and H. J. Schulze, Nucl. Phys. A **914**, 332 (2013).
- [42] T. Suzuki et al, Phys. Lett. B **597**, 263 (2004).
- [43] M. Agnello et al. , Phys. Rev. Lett. **94**, 212303 (2005).
- [44] M. Agnello et al. , Phys. Lett. B **654**, 80 (2007).
- [45] T. Yamazaki et al, Phys. Rev. Lett. **104**, 132502 (2010).
- [46] E. Oset, and H. Toki, Phys. Rev. C **74**, 015207 (2006).
- [47] V. K. Magas et al, Phys. Rev. C **74**, 025206 (2006).
- [48] V. K. Magas, E. Oset, and A. Ramos, Phys. Rev. C **77**, 065210 (2008).
- [49] S. Ajimura et al., Nucl. Phys. A **914**, 315 (2013).
- [50] Y. Ichikawa et al., Few-Body Syst. **54**, 1191 (2013).
- [51] D. Gazda et al, Phys. Rev. C **77**, 045206 (2008).
- [52] B. D. Serot, J. D. Walecka, Adv. Nucl. Phys. **16**, 1 (1986).
- [53] W. J. Jiang, et al, Phys. Rev. C **72**, 024313 (2005).
- [54] P. Alberto et al, Phys. Rev. C **65**, 034307 (2002)
- [55] G. A. Lalazissis, J. König, and P. Ring, Phys. Rev. C **55**, 540 (1997).
- [56] J. N. Ginocchio, and D. G. Madland, Phys. Rev. C **57**, 1167 (1998).
- [57] M. M. Sharma and M. A. Nagaragian, Phys. Lett. B **312**, 377 (1993).